Cell, Vol. 112, 859–871, March 21, 2003, Copyright ©2003 by Cell Press

Structural Basis for the Autoinhibition of c-Abl Tyrosine Kinase

Bhushan Nagar,[1,7] Oliver Hantschel,[3,7] Matthew A. Young,[1] Klaus Scheffzek,[4] Darren Veach,[6] William Bornmann,[6] Bayard Clarkson,[6] Giulio Superti-Furga,[3,5,*] and John Kuriyan[1,2,*]

[1]Howard Hughes Medical Institute
Department of Molecular and Cell Biology
Department of Chemistry
University of California, Berkeley
[2]Physical Biosciences Division
Lawrence Berkeley National Laboratory
Berkeley, California 94720
[3]Developmental Biology Programme
[4]Structural and Computational Biology
European Molecular Biology Laboratory
[5]Cellzome AG
Meyerhofstrasse 1
69117 Heidelberg
Germany
[6]Memorial Sloan-Kettering Cancer Center
New York, New York 10021

Summary

c-Abl is normally regulated by an autoinhibitory mechanism, the disruption of which leads to chronic myelogenous leukemia. The details of this mechanism have been elusive because c-Abl lacks a phosphotyrosine residue that triggers the assembly of the autoinhibited form of the closely related Src kinases by internally engaging the SH2 domain. Crystal structures of c-Abl show that the N-terminal myristoyl modification of c-Abl 1b binds to the kinase domain and induces conformational changes that allow the SH2 and SH3 domains to dock onto it. Autoinhibited c-Abl forms an assembly that is strikingly similar to that of inactive Src kinases but with specific differences that explain the differential ability of the drug STI-571/Gleevec/imatinib (STI-571) to inhibit the catalytic activity of Abl, but not that of c-Src.

Introduction

The cellular form of the Abelson leukemia virus tyrosine kinase, c-Abl, is a relative of the Src family of tyrosine kinases. Its regulation has been a long standing enigma. c-Src, prominent in the history of cell signaling because of its relationship to the oncogene product v-Src, is controlled by an interaction between the Src homology 2 (SH2) domain of the protein and a phosphorylated tyrosine residue (Tyr-527) in the C-terminal tail (Thomas and Brugge, 1997). v-Src lacks the Tyr-527 phosphorylation site, and the catalytic activity of v-Src is unregulated. c-Abl possesses all the essential regulatory elements of c-Src except that c-Abl, like v-Src, lacks a phosphorylation site corresponding to Tyr-527 (Superti-Furga and Courtneidge, 1995). Nevertheless, the catalytic activity of c-Abl is properly regulated.

c-Abl consists of ~1150 residues (Van Etten, 1999). The N-terminal half of the protein includes an N-terminal "cap" of ~80 residues that is important for autoinhibition (Pluk et al., 2002) followed by an SH3 domain, an SH2 domain, and a tyrosine kinase domain (Figure 1A). With the exception of the N-terminal cap region, which is unique to c-Abl and the Abl-paralog Arg (*ABL2*), the N-terminal half of c-Abl resembles closely the Src family tyrosine kinases (Superti-Furga and Courtneidge, 1995). The C-terminal half of c-Abl includes binding elements for SH3 domains, nuclear localization and export signals, a DNA binding functionality, and an actin binding domain. Human cells express two splice variants of c-Abl, Abl 1a and Abl 1b, which differ only in the very N-terminal region. Abl 1b is myristoylated, whereas Abl 1a is not.

The inadvertent fusion of the gene encoding c-Abl with the breakpoint cluster region (BCR) gene results in the formation of a fusion protein, BCR-Abl, in which all of c-Abl is preserved without mutation, except for a small N-terminal region, upstream of the SH3 domain (Figure 1A). The fusion with BCR disrupts the internal control mechanism that keeps c-Abl in an inactive form, and the enhanced tyrosine kinase activity of the BCR-Abl protein results in the disease chronic myelogenous leukemia (CML) (for a recent review, see Sawyers, 2002).

The drug STI-571 is effective in the treatment of CML and blocks the kinase activity of BCR-Abl (Druker et al., 1996; Sawyers, 2002). Crystal structures of the isolated kinase domain of Abl show that STI-571 displaces ATP and traps an inactive conformation of the kinase domain (Nagar et al., 2002; Schindler et al., 2000). Strikingly, residues that interact with the drug are conserved in the Src kinases, but STI-571 does not inhibit the kinase activity of c-Src (Druker et al., 1996; Schindler et al., 2000). A simple explanation for this phenomenon is that Src is unable to adopt the particular conformation required for the binding of STI-571 (Nagar et al., 2002). However, Src and Abl are very closely related in sequence, and it is not clear why the distinct inactive conformations seen for their kinase domains cannot readily interconvert. The origin of the differential sensitivity toward STI-571 is therefore not completely understood.

Crystal structures of the Src kinases c-Src and Hck have been determined in the inactive and assembled states (Schindler et al., 1999; Xu et al., 1999) and that of the kinase domain of the Src kinase Lck in the phosphorylated active state (Yamaguchi and Hendrickson, 1996). The structure of the kinase domain of active Lck resembles that of the active forms of other Ser/Thr and tyrosine kinases (Huse and Kuriyan, 2002). Phosphorylation on Tyr-416 (chicken c-Src numbering) in the activation loop helps to maintain a conformation that allows access to the substrate binding site while properly positioning catalytic residues for phosphate transfer. Inactivation of the Src kinases requires the internal en-

*Correspondence: kuriyan@uclink.berkeley.edu (J.K.), superti@embl-heidelberg.de (G.S.-F.)
[7]These authors contributed equally to this work.

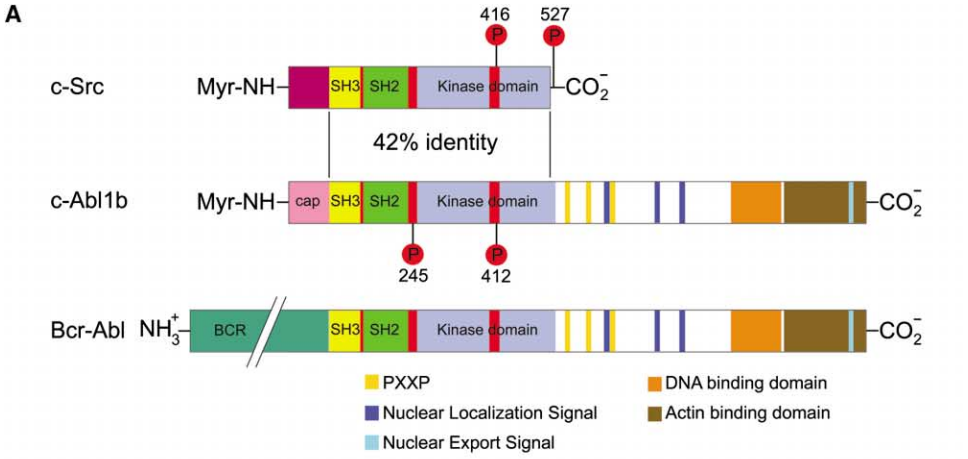

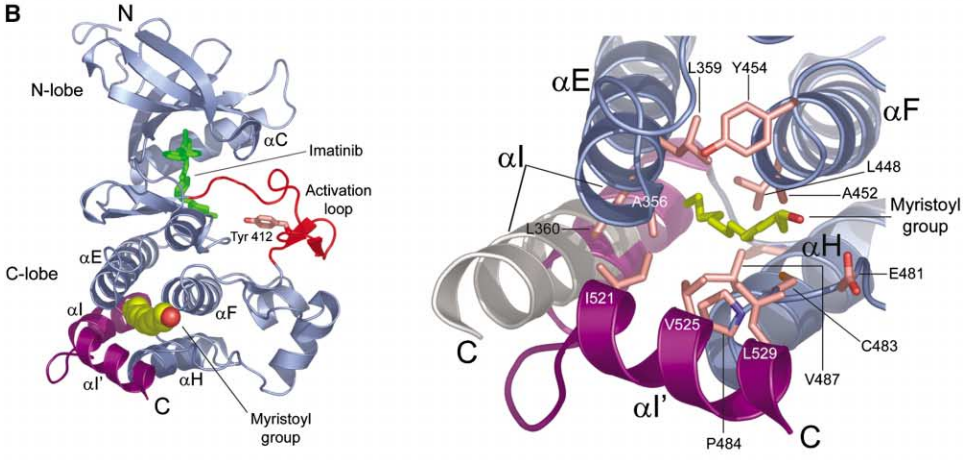

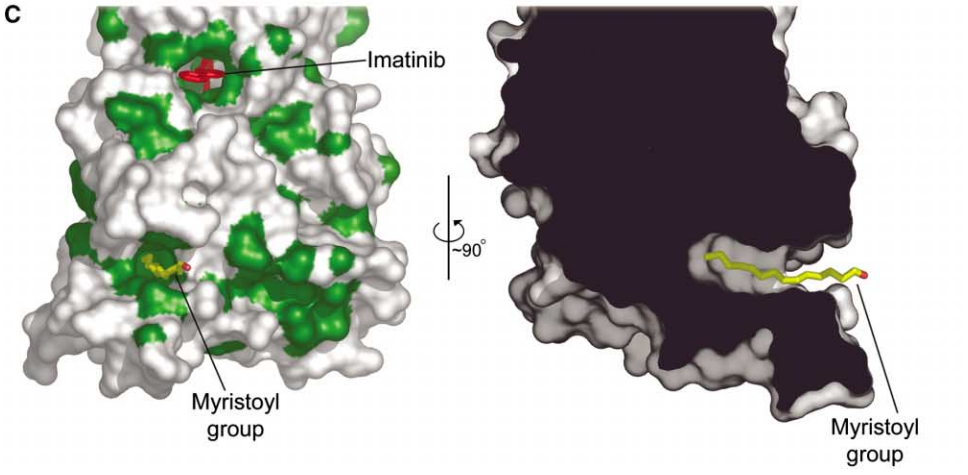

Figure 1. Structure of the c-Abl Kinase Domain

(A) Domain structure of c-Src, c-Abl 1b, and Bcr-Abl. Potential tyrosine phosphorylation sites are indicated with red circles and the residue number. Additional phosphorylation sites in the C-terminal region of Abl following the kinase domain are not shown.

(B) Left, structure of the kinase domain of c-Abl bound to a myristoylated peptide (Structure A). Only the myristoyl group is shown, since the rest of the peptide is disordered. Helices that change conformation upon myristoyl binding (αI and αI′) are colored purple. A closeup view of the myristoyl binding site is shown on the right. Superimposed and shown in gray is helix αI from the structure of the isolated kinase domain in the absence of the myristoyl group (PDB code 1M52).

(C) Molecular surface of $Abl^{248-534}$ (Structure A) in the same orientation as in (B). Hydrophobic sidechains are colored green. A cutaway rendition of the surface is shown on the right, rotated approximately 90° about the vertical axis with respect to the view on the left. Figures 1B–5 were prepared using PyMOL (DeLano, 2002).

gagement of the SH2 and SH3 domains to form the assembled state, triggered by the docking of the SH2 domain to the phosphorylated tyrosine residue located in the C-terminal tail of the protein (Tyr-527 in the conventional c-Src numbering).

As with the Src kinases, the SH3 and SH2 domains are both required for the proper regulation of c-Abl (Barila and Superti-Furga, 1998; Franz et al., 1989; Jackson and Baltimore, 1989; Muller et al., 1993), and it has been suggested that c-Abl adopts an assembled structure similar to that of the Src kinases when inactive (Pluk et al., 2002; Williams et al., 1997) despite the lack of a residue corresponding to Tyr-527 of c-Src. It has been shown recently that the N-terminal half of c-Abl is sufficient for maintenance of the inactive state (Pluk et al., 2002). In particular, the N-terminal cap region of c-Abl is essential for regulation, suggesting that the cap somehow compensates for the lack of a Src-like C-terminal phosphotyrosine. This has no precedent in the Src kinases, where the corresponding N-terminal unique region is crucial for membrane anchorage, but not for the regulation of kinase activity (Koegl et al., 1995).

There are significant differences in the structures of the Src and Abl kinase domains despite close similarity at the sequence level (47% identity) (Nagar et al., 2002). The major inactivating switch within the kinase domain of c-Abl is a large conformational change at the base of the activation loop, not seen in c-Src or Hck, which flips the positions of aspartate and phenylalanine side chains in a conserved Asp-Phe-Gly (DFG) motif (residues 400–402; Abl 1b numbering) (Nagar et al., 2002). The flipped conformation of the aspartate side chain prevents the coordination of the catalytically important magnesium ion at the active site. This conformational change in the DFG motif is inconsistent with a closure of the kinase domain that is seen in inactive c-Src and Hck, and the catalytic domain of c-Abl is essentially in the open conformations seen in active kinases. The binding of STI-571 requires this open conformation, as well as displacements in the DFG motif and the activation loop (Nagar et al., 2002). An important question is whether these distinctive conformational features of the isolated Abl kinase domain persist in the assembled state of the protein.

We now present crystallographic analyses of an autoinhibited fragment of c-Abl 1b and show that it adopts an assembled state, which is strikingly similar in general terms to that of the Src kinases, with the SH3 and SH2 domains docked onto the surface of the kinase domain that is distal to the active site. The internal docking of the SH2 domain requires the induction of a sharp bend in the C-terminal helix at the base of the kinase domain. This conformational change is triggered by the binding of the N-terminal myristoyl group of the protein to the base of the kinase domain, and the generation of this interaction appears to be a primary role of the N-terminal cap region. Critical differences between c-Src and c-Abl in the way in which the SH2 domain docks onto the kinase domain are reflected in differences in the conformations of their kinase domains, which provides an explanation for the ability of STI-571 to bind preferentially to c-Abl over c-Src.

Results and Discussion

Structural Analysis of c-Abl

We initiated structural studies on a construct of human Abl 1b, spanning residues 1–531, which we refer to as c-Abl$^{1-531}$. Expression of this construct in baculovirus-infected insect cells produced a protein that was myristoylated but was extremely soluble, suggesting that the myristoyl modification was probably not exposed to solvent. Further investigation showed that a short myristoylated peptide interacts with the isolated catalytic domain of c-Abl with micromolar affinity (Hantschel et al., 2003 [this issue of *Cell*]).

We determined three crystal structures that have shed light on the regulatory mechanism of c-Abl (Table 1). Two small molecule inhibitors of kinase activity, STI-571 and PD166326, proved helpful for crystallization, but we do not discuss them in detail here since the essential features of their interaction with the kinase domain have been described (Nagar et al., 2002; Wisniewski et al., 2002). We first determined, at 1.75 Å resolution, the structure of the isolated kinase domain of c-Abl bound to STI-571 and to a myristoylated peptide corresponding to the N-terminal 16 residues of Abl 1b (Structure A). We also crystallized myristoylated c-Abl$^{1-531}$ bound to PD166326 and determined its structure at 3.4 Å resolution (Structure B). Finally, we determined the structure of a construct of c-Abl spanning residues 46–534 (c-Abl$^{46-534}$, beginning at the first exon that is common to the 1a and 1b spliceforms and continuing until the end of the kinase domain), to which we added PD166326 and myristic acid during purification and crystallization, respectively. This allowed the determination of the crystal structure of an assembled, myristate bound form of c-Abl at 1.8 Å resolution (Structure C).

Myristoyl-Induced Conformational Changes in the Kinase Domain

The myristoyl group penetrates deep into the base of the C lobe of the kinase domain in Structure A (Figure 1B). When the myristoyl group is absent, the C-terminal helix of the kinase domain, αI, extends from residue Ser-504 to Ser-522, with subsequent residues being disordered (Nagar et al., 2002). In the presence of the myristoyl group, helix αI breaks at residue Phe-516, with residues Phe-516 to Ser-519 forming a four-residue turn, which produces a $\sim$90° degree bend in the direction of the polypeptide backbone before it forms another helix, αI′ (Figure 1B). The new helix αI′ consists of three turns, spanning residues Ser-520 to Lys-531.

The myristoyl group is bound in a deep pocket formed by hydrophobic side chains emanating from helices αE (Ala-356, Leu-359, Leu-360), αF (Leu-448, Ala-452, Tyr-454), αH (Cys-483, Pro-484, Val-487, and aliphatic atoms of the Glu-481 side chain), and the new helix, αI′, (Ile-521, Val-525, Leu-529) (Figure 1B). The inner portion of the binding site is approximately 10 Å deep and provides a snug fit for the terminal nine carbon atoms of the myristoyl group (C6 to C14) (Figure 1C). The remaining carbon atoms of the myristoyl group (C2 to C5) lie in the broader opening of the pocket where the side chains of Val-525 and Leu-529 from the induced helix αI′ form a hydrophobic shelf for the myristoyl group. Approxi-

Table 1. Data Collection and Refinement Statistics

	Structure A ($Abl^{248-534}$)[b]	Structure B (Abl^{1-531})[c]	Structure C (Abl^{46-534})[c]
Data Collection			
Beamline	ESRF ID14.1	ALS 8.2.1	ALS 8.2.2
Resolution (Å)	30–1.7 (1.8–1.7)	75–3.4 (3.52–3.4)	38–1.8 (1.86–1.8)
Measured reflections (#)	268488	105428	360273
Unique reflections (#)	61592	17250	50963
Data Redundancy	4.4	6.1	7.1
Data Completeness (%)	92.9 (75.8)	95.1 (91.4)	99.9 (100.0)
R_{sym} (%)[a]	9.0 (50.9)	8.1 (46.5)	5.7 (58.4)
I/sig I	9.4 (2.8)	19.7 (3.4)	29.6 (3.5)
Refinement			
R factor/R free[d]	21.0/24.2	30.6/31.5	19.6/22.1
Free R test set size (#/%)	2886/5.0	1106/6.8	2966/6.0
Number of protein atoms	2329	6584	3613
Number of heterogen atoms	104	73	45
Number of solvent atoms	233	0	276
Rmsd bond lengths (Å)	0.008	0.010	0.009
Rmsd bond angles (°)	1.4	1.6	1.5
Rmsd B factors (Å²) (main chain/side chain)	1.39/1.97	3.45/5.53	1.53/2.35

[a] $R_{sym} = \Sigma|I - \langle I \rangle|/\Sigma I$, where I is the observed intensity of a reflection, and $\langle I \rangle$ is the average intensity obtained from multiple observations of symmetry-related reflections.
[b] Data processed with XDS/XSCALE.
[c] Data processed with DENZO/Scalepack.
[d] For refinement, the high-resolution cutoff used for Structure A was 1.75 Å and the low-resolution cutoff used for Structure B was 30.0 Å.

mately 500 Å² is buried between the protein and the myristoyl group. There is no electron density for the peptide portion of the N-terminal segment, suggesting that specific interactions between the kinase domain and the first few residues of the N-terminal cap of Abl 1b may be limited. This is consistent with the results of mutations in the N-terminal cap of Abl 1b (Hantschel et al., 2003).

The conformation of helix αI has been determined in several crystallographically independent structures of the isolated kinase domain of c-Abl in the myristoyl-free form (Nagar et al., 2002; Schindler et al., 2000). In each case, the conformation of helix αI is essentially the same and corresponds to the unbent and extended conformation (Figure 1B) also seen in one of the two kinase domains in the crystal structure of $c\text{-}Abl^{1-531}$ from which the myristoyl group had been displaced during crystallization (see below). The bent conformation of the C-terminal helix is now observed in four crystallographically independent views: two in the structure of the isolated kinase domain complexed to the myristoylated peptide (Structure A), one in the crystal structure of myristoylated $c\text{-}Abl^{1-531}$ (Structure B), and one in the structure of $c\text{-}Abl^{46-534}$, to which myristate was added in *trans* (Structure C). We conclude that the kinase domain of c-Abl undergoes a well-defined transition in which the C-terminal helix of the kinase domain switches conformations such that helix αI is either straight or sharply bent and that the myristoyl group is capable of inducing and stabilizing the bent conformation without the assistance of the SH2 and SH3 domains. Comparison with the structure of the kinase domain without myristate and bound to STI-571/Gleevec/imatinib or PD173955 (Nagar et al., 2002) indicates that the presence of the small molecule inhibitors is unlikely to influence the myristate binding site, which is located ~25 Å from the inhibitors.

The residues that make up the myristate binding site in c-Abl are all strictly conserved in the Abl paralog Arg, suggesting that the myristoyl group of Arg 1b may also bind to the kinase domain. The general structure of the base of the kinase domain is conserved between Abl and the Src kinases. However, several residues that line the myristate binding site in c-Abl are replaced in c-Src by bulkier residues, which block the binding site (e.g., Ala-356, Ala-452, Gly-482, and Val-487 in c-Abl are replaced in c-Src by Leu, Thr, Glu, and Leu). This suggests that the myristoyl group of Src is unlikely to interact with the kinase domain.

Crystallographic Analysis of the Inactive and Assembled Form of c-Abl

Crystals of the myristoylated and unphosphorylated $c\text{-}Abl^{1-531}$ complexed to PD166326 are obtained readily but diffract X-rays weakly (3.4 Å). There are two molecules of c-Abl in the asymmetric unit of these crystals, one of which corresponds to an inactive and assembled form (Structure B). Unexpectedly, only the kinase and SH2 domains of the second molecule could be localized in electron density maps. The second kinase domain shows no evidence for a bound myristoyl group, and its C-terminal helix αI is in the straight conformation corresponding to myristoyl-free c-Abl.

The SH2 domain of the second c-Abl molecule is located on top of the kinase domain so that it interacts closely with the upper surface of the β sheet in the N lobe. The significance of this unusual SH2-kinase domain interaction is not clear, and there is no electron density for the SH3 domain or for the linker connecting the kinase domain to the SH2 domain. This second c-Abl assembly has very high temperature factors (200 Å²), and its structure cannot be refined or analyzed in detail. Mass spectrometric analysis of the protein samples

used for crystallization indicate that the protein is intact and completely myristoylated, and it is not clear why this molecule is in a disassembled state.

Despite the limited resolution of the X-ray data, we were able to generate a reasonably accurate model for the assembled c-Abl molecule by using the known structures of the SH3, SH2, and kinase domains (Nagar et al., 2002; Nam et al., 1996). As in c-Src, the linker connecting the SH2 domain to the kinase domain (SH2-kinase linker) forms an internal binding site for the SH3 domain. The SH2 domain is docked onto the distal surface of the kinase domain, which it approaches much more closely than in c-Src or Hck. Despite the general similarities between c-Abl and the Src kinases, the kinase domain of c-Abl retains the conformation seen earlier in structures of the isolated and unphosphorylated kinase domains, which is distinctly different from the conformation of the kinase domain in c-Src (Nagar et al., 2002; Schindler et al., 2000).

There is no clearly interpretable electron density for the ~80 residue N-terminal cap region for the assembled c-Abl molecule, although there is some evidence for localized interactions with the SH3-SH2 assembly. Strong peaks in electron density maps, consistent with the presence of unmodeled peptide segments, are seen in the vicinity of the N-terminal region of the SH3 domain and also at the junction of the SH3 and SH2 domains with the SH2-kinase linker (indicated schematically in Figure 4). The low resolution and disconnected nature of these electron density features preclude a detailed molecular analysis. Nevertheless, we conclude that limited regions of the N-terminal cap, probably the functionally important residues Lys-70 and Leu-73 (Hantschel et al., 2003), interact with the SH2 and SH3 domains, perhaps further strengthening the connections between them and the kinase domain.

Analysis of the Assembled c-Abl Structure at 1.8 Å Resolution

The crystal structure of c-Abl$^{46–534}$, complexed to PD166326 and myristate (added in *trans*) is very similar to Structure B, except that it is resolved at high resolution (Figure 2A). There is no electron density for the portion of the N-terminal cap included in this construct (residues 46–82), and the modeled structure begins at the first residue of the SH3 domain.

There is particularly good agreement between c-Abl and c-Src in the SH3-SH2 subassembly (Figure 2B). Least-squares superimposition of the SH3-SH2 unit, including the SH3-2 connector, results in a root mean square (rms) deviation in Cα atoms of 1.2 Å between c-Abl and c-Src for 151 structurally aligned residues. If the SH2-kinase linker and the N lobe are included in the structural comparison, the rms deviation in Cα atoms is 1.7 Å. This close structural correspondence between c-Src and c-Abl does not extend to the C lobe of the kinase domain, which is rotated outwards in c-Abl by about 20°, so that it approaches the SH2 domain more closely. Given the preservation of the SH3-linker-N lobe interface, the opening up of the N lobe with respect to the C lobe is correlated with a movement of the SH2 domain of c-Abl toward the C-terminal lobe of the kinase, resulting in a significantly tighter SH2-kinase interface than in c-Src. The total surface area buried at the SH2-kinase interface is 920 Å^2 in c-Abl, compared to 500 Å^2 and 460 Å^2 in c-Src and Hck, respectively.

Interestingly, certain aspects of the structure of c-Abl are more similar to corresponding elements in c-Src than in the Src kinase Hck (Schindler et al., 1999; Xu et al., 1999). When Cα atoms in the SH3-SH2 unit, the SH2-kinase linker, and the N lobe are superimposed between c-Abl and Hck, 254 residues are aligned with a rms deviation of 2.2 Å, compared to 1.7 Å for the c-Src alignment. Hck contains an intact Pro-x-x-Pro (PxxP, where x is any residue) motif in the SH2-kinase linker (Figure 3A). The two proline residues pack against the SH3 domain, and the SH2-kinase linker forms a nearly regular polyproline type II helix, the standard recognition element for SH3 domains (Kuriyan and Cowburn, 1997). The second proline residue of the PxxP motif is replaced in c-Abl and c-Src by Tyr-245 and Gln-253, respectively. In c-Abl and c-Src the linker is distorted so that Tyr-245 (Figure 2A) and Gln-253 point away from the surface of the SH3 domain, packing against the kinase domain instead (Figure 3A). An interesting question is whether these structural differences are correlated with a significant difference in the ease of activation of c-Src or c-Abl by SH3 displacement when compared to Hck.

Tyr-245 is a site of regulatory control in c-Abl, with phosphorylation of this residue potentiating catalytic activity (Brasher and Van Etten, 2000). The distortion of the SH2-kinase linker from ideal polyproline type II geometry results in the packing of Tyr-245 in a hydrophobic crevice formed by the side chains of Lys-313 and Pro-315 of the kinase domain. Clearly, phosphorylation of Tyr-245 would dislodge it from this nonpolar site and disrupt the assembled structure, consistent with the high levels of activity observed upon phosphorylation of Tyr-245 in c-Abl (Brasher and Van Etten, 2000).

The assembled structure is consistent with a number of mutations made in the SH3 domain of c-Abl. For example, mutations in the "RT-loop" of the SH3 domain (residues 91–99) do not result in the activation of c-Abl (Brasher et al., 2001). This result is consistent with the lack of extensive contact between the SH2-kinase linker and the RT-loop due to the replacement of the second proline of the PxxP motif in the SH2-kinase linker of c-Abl by Tyr-245 (Figure 3A). Glu-117 and Lys-313 have been implicated in the autoinhibition of c-Abl activity and predicted to form a salt bridge (Barila and Superti-Furga, 1998), and the structure confirms this interaction. Replacement of Ser-94 in c-Abl by arginine was shown to suppress activation relative to wild-type Abl (Brasher et al., 2001), and this position is occupied in c-Src by an arginine residue that interacts with carbonyl groups presented by the SH2-kinase linker, suggesting that the arginine in the S94R mutation in c-Abl might form similar interactions.

Docking of the SH2 Domain Requires a Sharp Bend in the C-Terminal Helix of the Kinase Domain and Is Incompatible with SH2 Ligation

The coupling between the SH2 domain and the kinase domain in both c-Src and Hck relies on the phosphorylated tyrosine residue in the C-terminal tail. In c-Abl, in contrast, the SH2 domain is docked closely onto the

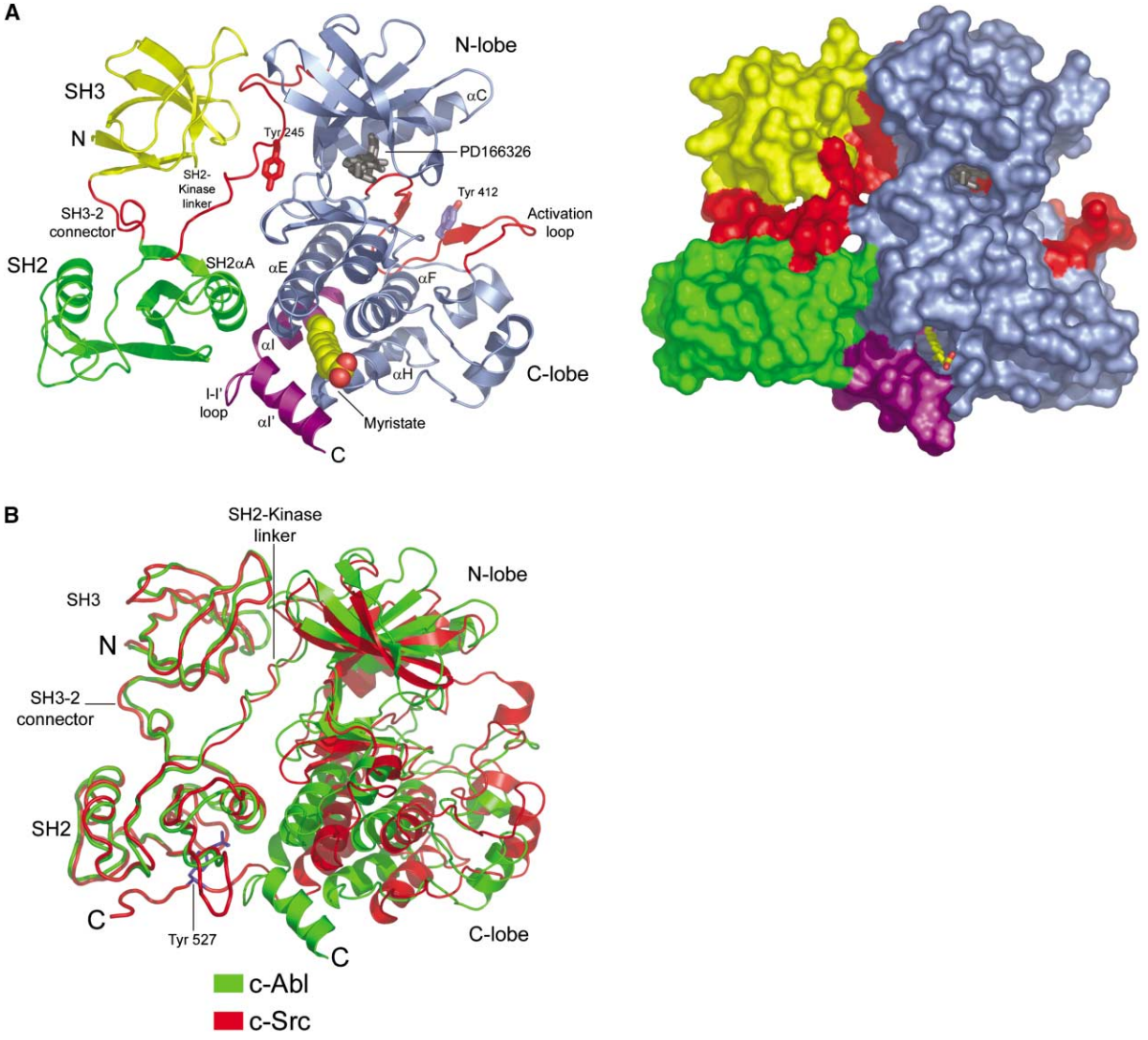

Figure 2. Structure of Assembled c-Abl

(A) Ribbon and surface representations of c-Abl (Structure C).

(B) Superposition of the structure of c-Src (red; PDB code 2SRC) onto the SH3 and SH2 domains (residues 83–233) of Abl[46–534] (Structure C; green).

kinase domain through an interlocking network of hydrogen bonding interactions (Figure 3B). These interactions can only occur upon the restructuring of the C-terminal helix αI, as induced here by myristate binding.

The carboxyl group of Glu-157 of the SH2 domain is located near the positive pole of the helix dipole of αI′, the orientation of which is dependent on the presence of myristate. Other interactions involve the packing of the N-terminal helix of the SH2 domain, SH2-αA, against helices αE and αI of the kinase domain. The side chains that lie along the outer edge of SH2-αA interact with the kinase domain through a series of direct hydrogen bonding interactions. Ser-152, located at the N-terminal end of the helix, makes a hydrogen bond with Glu-513 of the kinase domain. Arg-153, a side chain that interacts with the phosphotyrosine residue of target peptides, makes two hydrogen bonds with the backbone carbonyl groups of residues 516 and 517 in the myristoyl-induced I-I′ loop. Asn-154 makes a hydrogen bond with the backbone carbonyl group of Glu-513, an interaction that knits the domains together by positioning the Glu-513 side chain appropriately for interaction with the SH2 domain.

A key set of interactions is made by Tyr-158 of the SH2 domain, the aromatic ring of which stacks, almost perfectly, with that of Tyr-361 within helix αE of the kinase domain. The hydroxyl group of Tyr-158 forms a hydrogen bond with the backbone carbonyl group of Asn-393 of the kinase domain, which in turn forms a hydrogen bond with Asn-240, located at the beginning of the interaction between the SH2-kinase linker and the SH3 domain. The close juxtapositioning of the SH2 and kinase domains in c-Abl therefore includes interactions that extend into the SH3-kinase interface, in a manner not seen in the Src-kinases (Figure 3B).

Without myristate, the C-terminal helix of the kinase domain, αI, extends out of the main body of the kinase

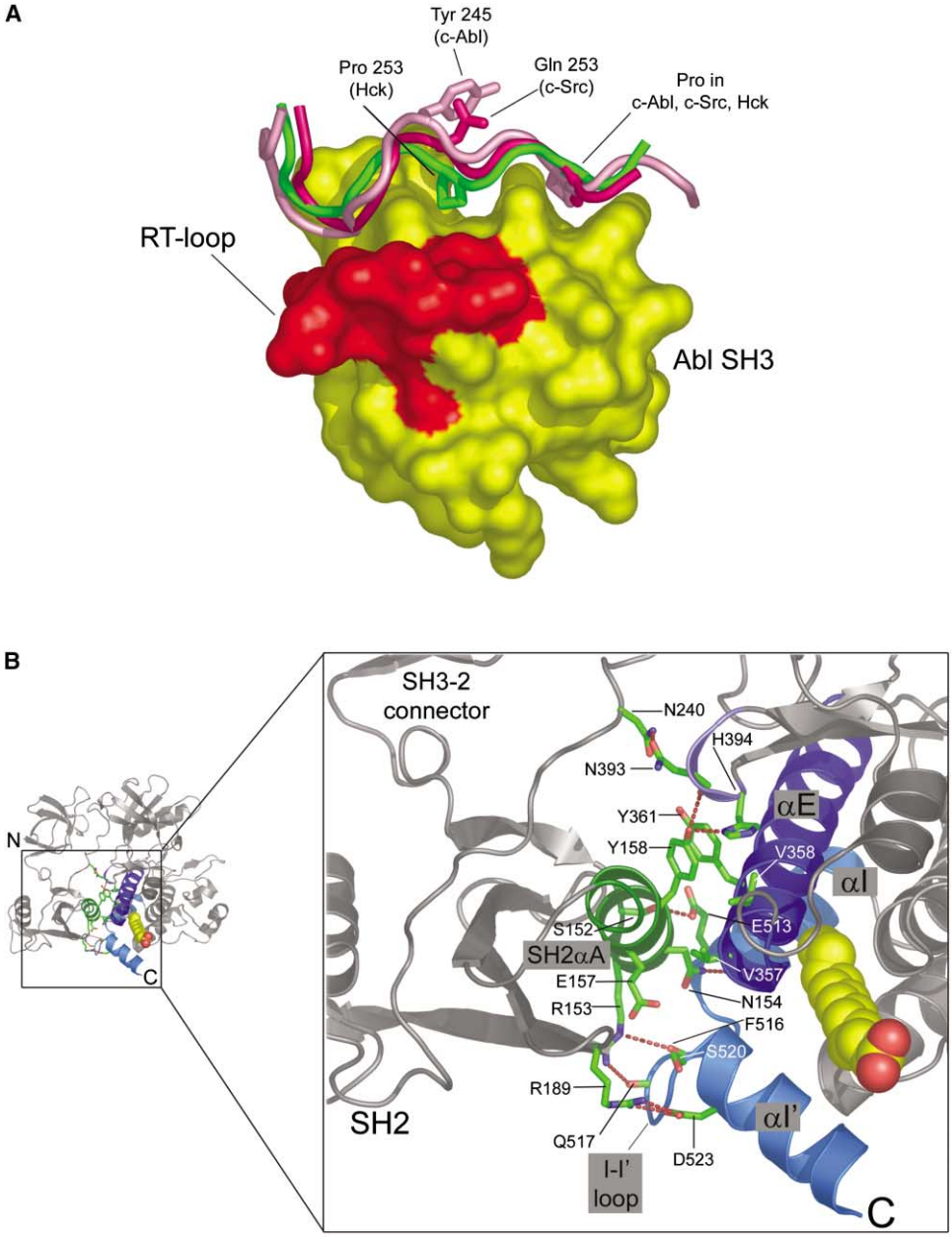

Figure 3. SH3 and SH2 Interactions

(A) Surface rendition of the Abl SH3 domain of Abl$^{46-534}$ (Structure C; yellow) bound to the SH2-kinase linker region (pink). The corresponding SH2-kinase linker regions from c-Src (magenta) and Hck (green) are superimposed. Only the SH3 domain was used in the superimposition.
(B) SH2-kinase interface region of Abl$^{46-534}$ (Structure C).

domain and the side chain of Phe-516, and subsequent residues of helix αI occlude the SH2 docking site on the kinase domain (Figure 4). This suggests that a gating mechanism is at work within the kinase domain in which the myristate plays a role in stabilizing the internal docking of the SH2 domain.

The orientation of the polypeptide backbone of phosphopeptides bound to SH2 domains is determined quite precisely by hydrogen bonding interactions between the SH2 domain and the backbone of the phosphopeptide (Kuriyan and Cowburn, 1997). Arg-153 in the SH2 domain is an important element in phosphopeptide recognition, and in the assembled c-Abl structure, the conformation of Arg-153 is not compatible with phosphotyrosine interaction. In addition, the I-I′ loop physically blocks the binding site for the residues at the −1 and −2 positions of an SH2 bound phosphopeptide. The peptide chain could not rearrange so as to avoid collision with the I-I′ loop while maintaining the interactions that hold the phosphotyrosine residue in place (Figure 5).

Rigidity of the SH3-SH2 Assembly and Implications for Catalytic Control

Given the close correspondence of the SH3-SH2 units of c-Src and c-Abl, we looked to see whether the dynamical

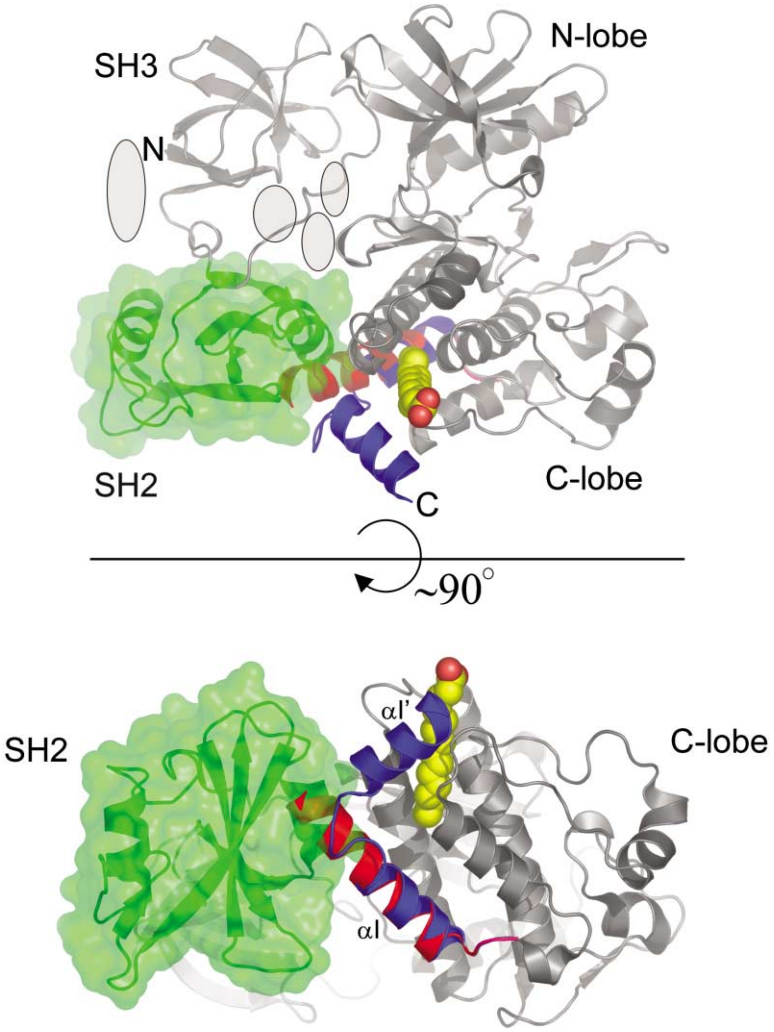

Figure 4. SH2 Gating Mechanism

Ribbon and surface representation of Abl$^{46–534}$ (Structure C) depicting the clash that occurs between helix αI in the myristoyl unbound form and the SH2 domain. Helix αI from the structure of the isolated kinase domain in the absence of myristoyl (PDB code 1M52) is colored red and the new helices (αI and αI′) formed upon binding of myristate are colored blue. Shown in shaded gray ellipses are regions that contain isolated patches of unmodeled electron density, potentially due to residues from the N-terminal cap region.

properties of the SH3 and SH2 domains of assembled c-Abl resemble that of c-Src and Hck. A total of four molecular dynamics simulations were carried out to a length of 4 ns each. Two of these started from crystal structures of assembled c-Abl and two from a variant structure in which three residues in the SH3-2 connector are replaced by glycine (S140G/L141G/E142G) (see Experimental Procedures). The first two (simulations one and two) were initiated from the low-resolution structure of the myristoylated c-Abl$^{1–531}$ (Structure B), and the two others (simulations three and four) were initiated from the high-resolution structure of c-Abl$^{46-534}$ (Structure C). The assembled structures were stable over the simulation period of 4 ns, with rms deviations in Cα positions of ~1.5–2.0 Å from the refined high-resolution crystal structure of c-Abl$^{46–534}$. The rms deviation in Cα positions for the average structure from the simulation of c-Abl$^{46–534}$ is 1.2 Å with respect to the crystal structure. The rms deviation of the average structure of the c-Abl$^{1-531}$ simulation relative to the high-resolution crystal structure of c-Abl$^{46–534}$, which was obtained after the simulation was completed, is 1.5 Å.

These simulations extend over too short a timescale for large-scale conformational transitions to occur spontaneously, but as for our previous simulations of c-Src and Hck, we have found the analysis of dynamical correlations in atomic positions to be informative (Young et al., 2001). As before, we analyze the movements of Cα atoms by reorienting each instantaneous structure in the dynamical trajectory onto a single frame of reference and then calculating the standard correlation coefficient between fluctuations in the positions of pairs of Cα atoms (Young et al., 2001). An analysis of the correlated motions within the structure of assembled c-Abl reveals strong dynamic coupling between the motions in the N lobe of the catalytic domain and the SH3 domain. This coupling extends into the SH2 domain via the SH3-2 connector. Cα atoms with cross correlation coefficients of greater than 0.75 in simulation three are connected with red lines in Figure 6A. These correlation coefficients are calculated by using the C lobe of the kinase as a frame of reference, which removes motions that are highly correlated to those of the C lobe of the kinase. For this reason, the SH2 domain appears unconnected to the kinase domain in the illustrations in Figure 6. Correlation coefficients calculated using the SH3 domain and the N lobe of the kinase as a frame of reference reveal an extremely tight coupling between the SH2 do-

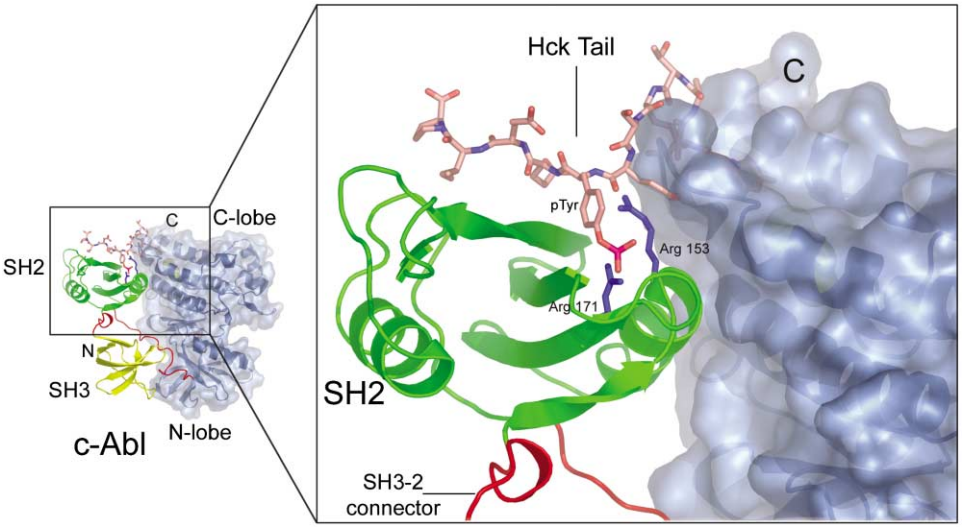

Figure 5. Blockage of Phosphorylated Peptide Binding

Ribbon and surface representation of Abl$^{46-534}$ (Structure C), illustrating that the SH2 peptide binding site is partially occluded when docked onto the kinase domain in assembled c-Abl. The tail peptide from Hck is shown bound to c-Abl using only the SH2 domains for superimposition.

main and the kinase domain (data not shown). Similar results are obtained for simulation one.

The residues connecting the SH3 and SH2 domains in c-Abl adopt a strikingly similar structure to that seen in the Src-family kinases, stabilized by a network of hydrogen bonds. Results of a correlation analysis of simulation four of assembled c-Abl with the glycine mutations in the SH3-2 connector are shown in Figure 6B, calculated as for the simulation of the protein with the wild-type connector sequence. The turn conformation of the SH3-2 connector shows increased flexibility in the simulation of this mutant variant of c-Abl. As a consequence, there is a reduction in the correlation of the motions of the SH2 and SH3 domains with the N lobe of the kinase domain and with each other. Similar results are obtained in simulation two. As for c-Src and Hck, the introduction of glycine residues in the c-Abl SH3-2 connector clearly breaks the rigidity of the assembly in the simulations, predicting that c-Abl bearing the triple glycine mutant will be active (Hantschel et al., 2003).

Conclusions

The similarity between the SH3-SH2 assemblies in c-Abl and c-Src contrasts with the differences in the conformations of the kinase domains in the inactive states of these proteins. In both c-Src and c-Abl, inactivation is coupled with "in/out" conformational transitions deep within the mouth of the kinase domain. These transitions are different in the Src kinases, where it involves helix αC, and c-Abl, where the DFG motif in the activation loop is flipped, but in both cases the transition from inactive to active would require the mouth of the kinase domain to open or flex. A plausible mechanism for the action of the SH2 and SH3 domains is that by forming a rigid clamp they prevent or dampen such breathing movements of the kinase domain (Williams et al., 1997; Young et al., 2001).

Rigidity in the SH3-SH2 unit contrasts with the results of NMR analyses of the isolated SH3-SH2 unit of c-Abl, which have demonstrated that the domains are flexible relative to one another in solution (Fushman et al., 1999). These apparently conflicting views of the SH3-SH2 unit can be reconciled by considering our molecular dynamics simulations of assembled c-Src and Hck (Young et al., 2001), and of c-Abl, which suggest that the connector between the SH3 and SH2 domains forms an "inducible snap-lock," adopting a rigid structure when the SH3 and SH2 domains are internally liganded but becoming flexible when these domains are released. The rigidity of the SH3-SH2 unit appears to be an essential component of the autoinhibitory mechanism, and the introduction of flexibility into the linker (by mutating three residues to glycine) was shown to activate c-Src in vivo (Young et al., 2001) (see Hantschel et al., 2003, for a mutational analysis of the SH3-2 connector in c-Abl).

The unexpected structural correspondence between c-Abl and c-Src in the SH2-SH3 subassembly rather than in the kinase domain helps explain the apparently paradoxical selectivity of STI-571 for c-Abl over c-Src. Our structural analysis shows that the formation of a structurally conserved and rigid SH2-SH3 clamp in these two proteins results in the kinase domain adjusting its conformation so as to accommodate the distinct mechanisms of SH2-kinase domain docking. Thus, c-Abl has its kinase domain in an open conformation with the DFG motif in the activation loop flipped, while c-Src does not. These distinctive features of the inactive kinase domain have been shown previously to be required for STI-571 binding (Nagar et al., 2002; Schindler et al., 2000), and our new results link them to the mechanism of autoinhibition by the SH2 and SH3 domains. Our structures of assembled and inactive Abl are consistent with the results of an in vitro screen for STI-571-resistant mutants of BCR-Abl, which revealed that the cap and SH3 and SH2 domains are important for the recognition of STI-571 (Azam et al., 2003 [this issue of *Cell*]).

The discovery of a myristoyl-triggered conformational

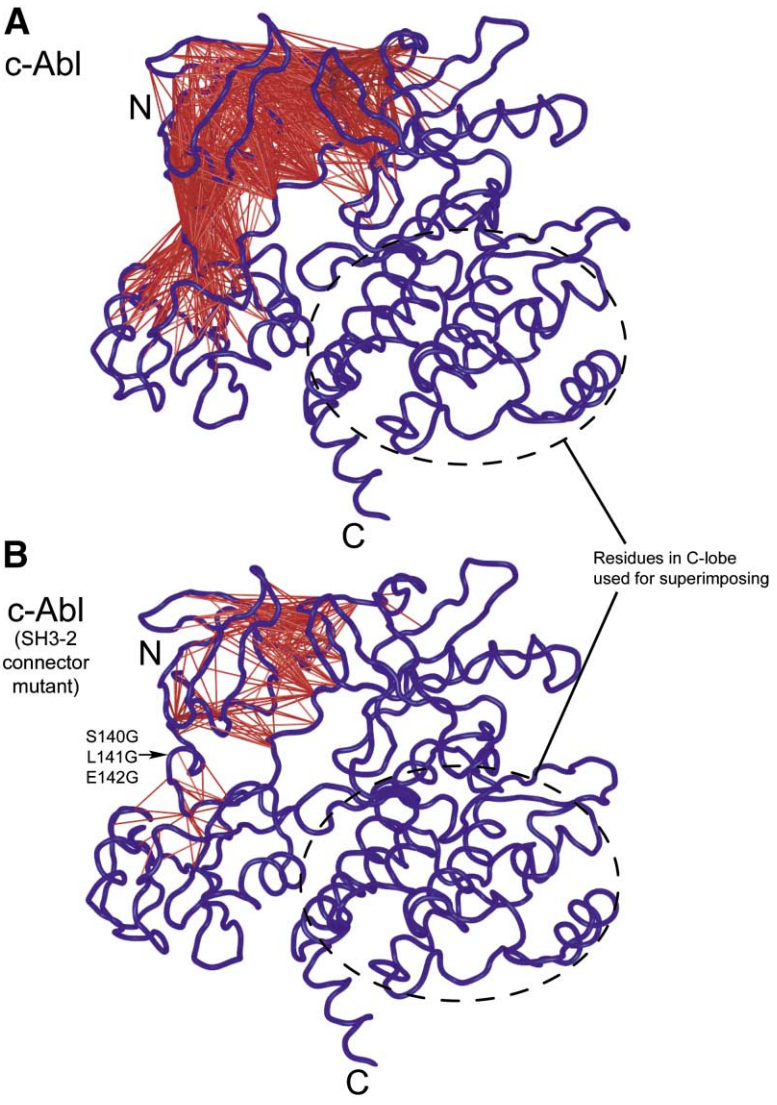

Figure 6. Schematic Diagram Indicating the Most Strongly Correlated Pairs of Cα Atoms in c-Abl$^{46-534}$ (Structure C) Computed from Molecular Dynamics Simulations

A dynamic cross correlation matrix was computed after superimposing each structure on the C lobe of the kinase domain. Data were computed over the 3.5 ns time period between 0.5 and 4.0 ns. Red lines connect Cα atoms in the structure which have cross-correlation coefficients of greater than 0.75. (A) Correlation coefficients from a simulation of the wild-type protein. (B) Cross correlations for a simulation of a S140G/L141G/E142G triple mutant of c-Abl. Data were analyzed over the same 0.5 ns to 4.0 ns time period. Both simulations were initiated from the high resolution structure of c-Abl (Structure C).

switch in the kinase domain was completely unexpected. One example of a soluble and myristoylated protein kinase of known three-dimensional structure is the cAMP dependent protein kinase PKA, where the regulatory RII subunit switches the N-terminal myristoyl modification of the catalytic domain from a kinase-bound state to a form that is released for interaction with membranes (Gangal et al., 1999). The myristoyl group is bound in a hydrophobic pocket located between the unique N-terminal helix of PKA and the two lobes of the kinase domain, and the details of the recognition of the myristoyl modification appear to be unrelated to that seen in c-Abl.

The myristoyl-induced conformational change in c-Abl is reminiscent of the structural changes induced in steroid/nuclear hormone receptors by the binding of agonists. In these receptors, C-terminal α helices reorganize from a more or less straight conformation in the unliganded receptor to one in which the polypeptide chain bends sharply and forms one face of the ligand binding pocket (Renaud et al., 1995). The common element in c-Abl, PKA, and the hormone receptors is the ability of polypeptide backbones of N- or C-terminal helical segments, tethered only at one end, to reorganize drastically without affecting the structural core of the protein. Although helix αI is not located in the C-terminal region of full-length c-Abl, we expect that the linker connecting the kinase domain to the region encoded by the last exon is flexible, allowing helix αI to change direction upon binding the myristoyl group.

It was known previously that mutations in the SH3 domain activate c-Abl, suggesting that SH3 displacement by peptide ligands might be one mode of activation, as for the Src kinases (Barila and Superti-Furga, 1998). The crystal structure of c-Abl shows that the formation of a phosphopeptide-SH2 complex would dislodge the SH2 domain from its docking site on the kinase domain. As shown in Hantschel et al. (2003), phosphopeptides can activate c-Abl by SH2 displacement. Thus, both c-Abl and the Src kinases may share a common mode of activation by displacement of their peptide binding modules.

Our crystallographic analyses, focused on the Abl 1b isoform, have revealed a role for the myristoyl group in

helping to stabilize the assembled and inactive form of c-Abl. The alternative spliceform Abl 1a is not myristoylated but is regulated normally (O.H. and G.S.-F., unpublished data), suggesting that Abl 1a contains additional interaction elements that compensate for the lack of the myristoyl group. The very N-terminal region of Abl 1a contains hydrophobic residues that are absent in Abl 1b, and one possibility is that these residues help induce the bend in helix αI that is essential for SH2 docking. Interactions that help pin the SH2 domain to the C lobe of the kinase, an essential aspect of the autoinhibitory mechanism, may also involve segments of the C-terminal region of full-length c-Abl that are known to play a role in regulation (Goga et al., 1993; Woodring et al., 2001).

The comparisons between c-Src and c-Abl now made possible by our crystal structures draws attention to the remarkable plasticity of the protein kinase domain, which is the only segment of the assembled and inactive states of these protein kinases that is seen to adapt its structure to the differing requirements of the autoinhibitory mechanisms. This emphasizes once more the opportunities that exist for developing small molecules that inhibit protein kinases specifically by exploiting the diversity of regulatory mechanisms that control protein kinase action.

Experimental Procedures

Protein Expression and Purification

Three different constructs of Abl were expressed: construct one (human c-Abl, spliceform 1b) encompasses the N-terminal 531 residues, including the myristoylation site, and is referred to as Abl^{1-531}. Construct two (mouse c-Abl) begins at the first common exon and extends to residue 534 and is referred to as Abl^{46-534}. There are only two differences within the sequence spanning the structural model (residues 83–531) between human and mouse c-Abl, Val-244 (human) to Ile (mouse) located in the SH2-kinase linker, and Asn-355 (human) to Ser (mouse) located on the surface of the C lobe of the kinase domain. Neither site is implicated in the regulatory mechanisms described here. Construct three (mouse c-Abl) is of the isolated kinase domain (residues 248–534, spliceform IV numbering) and was expressed and purified as described previously (Nagar et al., 2002; Schindler et al., 2000), and is referred to as $Abl^{248-534}$. Construct one was cloned into *pFastBac1* (Gibco BRL) with a C-terminal cleavage site for the Tobacco Etch Virus protease and a hexahistidine tag introduced by PCR. Construct two was cloned into a plasmid in which an N-terminal hexa-histidine tag is fused to the protein (*pFastbac HTa*, Gibco BRL).

To minimize heterogeneity due to autophosphorylation the catalytic domain in constructs one and two was rendered inactive by mutating the catalytic base Asp-382 to asparagine. Recombinant bacmid DNA containing the Abl insert was prepared according to the manufacturer's instructions (Bac-to-Bac expression system, Gibco BRL) and transfected into Sf9 cells. Baculovirus obtained from the transfection was then used to infect Sf9 cells grown in suspension to a density of 2.5×10^6 cells per ml at a multiplicity of infection of ten. Cells were grown for 48 hr, centrifuged, resuspended in buffer A (50 mM Tris/HCl [pH 8.0], 10% glycerol, 15 mM β-mercaptoethanol, and inhibitor cocktail pill [Roche]), flash frozen in liquid nitrogen, and stored at −80°C. Western blots with anti-phosphotyrosine antibody revealed that the protein was not tyrosine phosphorylated.

For a typical protein preparation, 4 liters of cells were thawed, lysed by sonication, and centrifuged at 17,000 rpm for 1 hr. The supernatant was filtered and loaded onto a 65 ml Q-Sepharose ion-exchange column equilibrated in buffer A. Protein was eluted from the column with 1 M NaCl. The total eluate was pooled and loaded onto a Ni-NTA column (Qiagen) equilibrated in 20 mM Tris/HCl [pH 8.0], 500 mM NaCl, 5% glycerol, 20 mM imidazole, and 5 mM β-mercaptoethanol. The protein was eluted with a linear imidazole gradient (20–500 mM), and fractions containing Abl were pooled.

The protein was incubated with calf-intestinal alkaline phosphatase (CiP, Roche) overnight at 20°C (5 U/mg recombinant protein), because ~80% of the protein was phosphorylated (presumably on Ser or Thr) as determined by mass spectrometry and native PAGE. A second Ni-column was used to remove the CiP. Abl-containing fractions were pooled and incubated with Tobacco Etch Virus protease overnight at 4°C in order to cleave the hexa-histidine tag from Abl. Next, inhibitor compound (PD166326) dissolved in DMSO was added at ~three times the molar protein concentration with constant stirring at 20°C. The inhibitor-protein complex was concentrated and loaded onto a Sephadex 200 gel filtration column (HiLoad 16/60, Pharmacia) equilibrated in 20 mM Tris/HCl (pH 8.0), 100 mM NaCl, and 5 mM DTT. Abl:inhibitor complex-containing fractions were pooled and diluted 1:4 to reduce the salt concentration, loaded onto a 1 ml Resource Q column (Pharmacia) and eluted with a linear salt gradient (20–250 mM NaCl). The major peak was pooled, concentrated to ~35 mg/ml and supplemented with 2–3 mM Triscarboxyethyl phosphine. For Abl^{46-534}, myristic acid was added in a ten-fold excess before concentrating. For $Abl^{248-534}$, myristoylated peptide was added in 1.5-fold excess before concentrating to ~20 mg/ml. The peptide sequence is Myr-GQQPGKVLGDQRRPSL and was synthesized at the Central Peptide Synthesis Unit of the German Cancer Research Centre in Heidelberg.

Synthesis of STI-571 and PD166326

STI-571 and PD166326 were synthesized and purified as described (Kraker et al., 2000; Zimmermann et al., 1997). The compounds were dissolved and stored as 20 mM aliquots in DMSO at −80°C until needed.

Crystallization and Data Collection

Using the hanging drop vapor diffusion method (0.6 μl protein solution + 0.6 μl reservoir solution), crystals of the Abl^{1-531} (construct one) grew in 0.8 M ammonium tartrate at 20°C (space group $C222_1$ with a = 112.9 Å, b = 147.4 Å, c = 153.4 Å and two molecules in the asymmetric unit). Crystals of Abl^{46-534} (construct two) grew in 20% (w/v) PEG 3350, 200 mM potassium nitrate at 20°C (space group $C222_1$ with a = 118.3 Å, b = 123.9 Å, c = 74.8 Å and one molecule in the asymmetric unit). Crystals of $Abl^{248-534}$ (construct three) grew in 22% (w/v) PEG 4000, 100 mM MES (pH 5.6), and 200 mM magnesium chloride at 4°C (space group P1 with a = 41.8 Å, b = 63.5 Å, c = 64.1 Å and two molecules in the asymmetric unit). All crystals were cryoprotected with the addition of 25% glycerol (v/v) and X-ray diffraction data were collected on crystals flash frozen in liquid nitrogen (Structure A) or initially frozen in liquid propane and stored in liquid nitrogen (Structures B and C) (Table 1). Data for Abl^{1-531} and Abl^{46-534} were integrated and scaled with DENZO and Scalepack (Otwinowski and Minor, 1997). Data for $Abl^{248-534}$ were processed with XDS (Kabsch, 1993).

Structure Determination and Refinement

All of the structures were solved with molecular replacement using AMoRe (Navaza, 1994). The search models used for Abl^{1-531} (Structure B) and Abl^{46-534} (Structure C) were PDB entries 2ABL (SH2, SH3 domains) (Nam et al., 1996) and 1M52 (kinase domain) (Nagar et al., 2002). The search model for $Abl^{248-534}$ (Structure A) was PDB entry 1IEP (Nagar et al., 2002). All models were subsequently refined with the programs CNS (Brunger et al., 1998) and O (Jones et al., 1991) (Table 1). After the refinement of Abl^{46-534} was completed, this model was used to complete the analysis of Abl^{1-531}. The refined Abl^{46-534} model was superimposed on the molecular replacement solution for the assembled molecule of Abl^{1-531}, and the positions of individual domains were optimized by rigid-body refinement. For the disassembled molecule, the kinase domain and SH2 domain of Abl^{46-534} were individually superimposed on the molecular replacement solution, followed by rigid-body refinement and application of an overall B factor to each domain.

Molecular Dynamics Simulations

Molecular dynamics simulations were carried out as described previously for c-Src and Hck (Young et al., 2001). Simulations of the

assembled Abl included residues 83–531, PD166326, and the myristoyl group. Two simulations (one and two) were carried out starting from the 3.4 Å structure of Abl^{1-531} bound to PD166326 (Structure B). Simulation two incorporated mutations in the SH3-2 connector. A second set of simulations (three and four) were carried out as before, except that the higher resolution structure (Structure C) was utilized as the starting conformation, and Asp-400 was simulated in a protonated (charge neutral) state. Asp-400 was determined to be in a protonated state based on the geometry of this sidechain in the high resolution structure and a comparison of this side chain orientation with the orientations sampled within the original two simulations, where it existed in a −1 charge state. AMBER parm99 force field parameters were utilized for the protein (Cornell et al., 1995). Parameters for the PD166326 inhibitor and the myristoyl group were generated using the Antechamber module in Amber version 7.0. Charges for these two molecules were assigned conforming to the BCC charge model using AM1 optimized geometries and potentials calculated in Mopac version 5.09mn.

A truncated octahedral geometry constructed of water extending a minimum of 10 Å beyond the protein was used for periodic boundary conditions. The net charge on the system was neutralized by the addition of 9 K^+ ions, and an additional 34 K^+/Cl^- ion pairs were added to the system to model an approximate 150 mM ionic strength environment. The simulation of the SH3-SH2 connector mutant was set up and carried out in an identical fashion, after manually introducing the following mutations: S140G/L141G/E142G. The simulations were carried out using the Sander module of Amber 7.0, using 16 processors on an IBM SP3 supercomputer located at the National Energy Research Scientific Computing Center (NERSC).

Acknowledgments

We thank Xiaoxian Cao and Huguette Viguet for excellent support of Sf9 cell culture; David King for mass spectrometry; Ruediger Pipkorn for peptide synthesis; Holger Sondermann, Patricia Pellicena, and Thomas Schindler for helpful discussions; and Stefania Gonfloni for initiating the collaborations between our groups. We are deeply grateful to Jose Marquez for crystallographic help and data collection at the ESRF in Grenoble. We thank Thomas Earnest and the staff at ALS for excellent crystallographic support. B.N. is supported by a fellowship from the Human Frontier Science Program. O.H. is supported by fellowships from the EMBL, the EMBO, and the Aventis Foundation. O.H. is a fellow of the German National Merit Foundation. Work in the G.S.F. laboratory is supported by the Cellzome AG and the EMBL. M.A.Y. is supported by fellowship DRG-1553 of the Damon Runyon Cancer Research Foundation and by a Career Award at the Scientific Interface from the Burroughs Wellcome Fund.

Received: January 16, 2003
Revised: February 19, 2003

References

Azam, M., Latek, R.R., and Daley, G.Q. (2003). Mechanisms of STI-571/imatinib resistance revealed by mutagenesis of *BCR-ABL*. Cell *112*, this issue, 831–843.

Barila, D., and Superti-Furga, G. (1998). An intramolecular SH3-domain interaction regulates c-Abl activity. Nat. Genet. *18*, 280–282.

Brasher, B.B., and Van Etten, R.A. (2000). c-Abl has high intrinsic tyrosine kinase activity that is stimulated by mutation of the Src homology 3 domain and by autophosphorylation at two distinct regulatory sites. J. Biol. Chem. *275*, 35631–35637.

Brasher, B.B., Roumiantsev, S., and Van Etten, R.A. (2001). Mutational analysis of the regulatory function of the c-Abl Src homology 3 domain. Oncogene *20*, 7744–7752.

Brunger, A.T., Adams, P.D., Clore, G.M., DeLano, W.L., Gros, P., Grosse-Kunstleve, R.W., Jiang, J.S., Kuszewski, J., Nilges, M., Pannu, N.S., et al. (1998). Crystallography & NMR system: A new software suite for macromolecular structure determination. Acta Crystallogr. D Biol. Crystallogr. *54*, 905–921.

Cornell, W.D., Cieplak, P., Bayly, C.I., Gould, I.R., Merz, K.M., Jr., Ferguson, D.M., Spellmeyer, D.C., Fox, T., Caldwell, J.W., and Kollman, P.A. (1995). A second generation force field for the simulation of proteins, nucleic acids, and organic molecules. J. Am. Chem. Soc. *117*, 5179–5197.

DeLano, W.L. (2002). The PyMOL User's Manual (San Carlos, CA: Delano Scientific).

Druker, B.J., Tamura, S., Buchdunger, E., Ohno, S., Segal, G.M., Fanning, S., Zimmermann, J., and Lydon, N.B. (1996). Effects of a selective inhibitor of the Abl tyrosine kinase on the growth of Bcr-Abl positive cells. Nat. Med. *2*, 561–566.

Franz, W.M., Berger, P., and Wang, J.Y. (1989). Deletion of an N-terminal regulatory domain of the c-abl tyrosine kinase activates its oncogenic potential. EMBO J. *8*, 137–147.

Fushman, D., Xu, R., and Cowburn, D. (1999). Direct determination of changes of interdomain orientation on ligation: use of the orientational dependence of 15N NMR relaxation in Abl SH(32). Biochemistry *38*, 10225–10230.

Gangal, M., Clifford, T., Deich, J., Cheng, X., Taylor, S.S., and Johnson, D.A. (1999). Mobilization of the A-kinase N-myristate through an isoform-specific intermolecular switch. Proc. Natl. Acad. Sci. USA *96*, 12394–12399.

Goga, A., McLaughlin, J., Pendergast, A.M., Parmar, K., Muller, A., Rosenberg, N., and Witte, O.N. (1993). Oncogenic activation of c-ABL by mutation within its last exon. Mol. Cell. Biol. *13*, 4967–4975.

Hantschel, O., Nagar, B., Guettler, S., Kretzschmar, J., Dorey, K., Kuriyan, J., and Superti-Furga, G. (2003). A myristoyl/phosphotyrosine switch regulates c-Abl. Cell *112*, this issue, 845–857.

Huse, M., and Kuriyan, J. (2002). The conformational plasticity of protein kinases. Cell *109*, 275–282.

Jackson, P., and Baltimore, D. (1989). N-terminal mutations activate the leukemogenic potential of the myristoylated form of c-abl. EMBO J. *8*, 449–456.

Jones, T.A., Zou, J.Y., Cowan, S.W., and Kjeldgaard, M. (1991). Improved methods for building protein models in electron density maps and the location of errors in these models. Acta Crystallogr. A *47*, 110–119.

Kabsch, W. (1993). Automatic processing of rotation diffraction data from crystals of initially unknown symmetry and cell constants. J. Appl. Crystallogr. *26*, 795–800.

Koegl, M., Courtneidge, S.A., and Superti-Furga, G. (1995). Structural requirements for the efficient regulation of the Src protein tyrosine kinase by Csk. Oncogene *11*, 2317–2329.

Kraker, A.J., Hartl, B.G., Amar, A.M., Barvian, M.R., Showalter, H.D., and Moore, C.W. (2000). Biochemical and cellular effects of c-Src kinase-selective pyrido[2, 3-d]pyrimidine tyrosine kinase inhibitors. Biochem. Pharmacol. *60*, 885–898.

Kuriyan, J., and Cowburn, D. (1997). Modular peptide binding domains. Annu. Rev. Biophys. Biomol. Struct. *26*, 259–288.

Muller, A.J., Pendergast, A.M., Parmar, K., Havlik, M.H., Rosenberg, N., and Witte, O.N. (1993). En bloc substitution of the Src homology region 2 domain activates the transforming potential of the c-Abl protein tyrosine kinase. Proc. Natl. Acad. Sci. USA *90*, 3457–3461.

Nagar, B., Bornmann, W.G., Pellicena, P., Schindler, T., Veach, D.R., Miller, W.T., Clarkson, B., and Kuriyan, J. (2002). Crystal Structures of the Kinase Domain of c-Abl in Complex with the Small Molecule Inhibitors PD173955 and Imatinib (STI-571). Cancer Res. *62*, 4236–4243.

Nam, H.J., Haser, W.G., Roberts, T.M., and Frederick, C.A. (1996). Intramolecular interactions of the regulatory domains of the Bcr-Abl kinase reveal a novel control mechanism. Structure *4*, 1105–1114.

Navaza, J. (1994). AMoRe: an automated package for molecular replacement. Acta. Crystallogr. A *50*, 157–163.

Otwinowski, Z., and Minor, W. (1997). Processing of X-ray diffraction data collected in oscillation mode. Methods Enzymol. *276*, 307–326.

Pluk, H., Dorey, K., and Superti-Furga, G. (2002). Autoinhibition of c-Abl. Cell *108*, 247–259.

Renaud, J.P., Rochel, N., Ruff, M., Vivat, V., Chambon, P., Gronemeyer, H., and Moras, D. (1995). Crystal structure of the RAR-gamma

ligand-binding domain bound to all-trans retinoic acid. Nature *378*, 681–689.

Sawyers, C.L. (2002). Disabling Abl-perspectives on Abl kinase regulation and cancer therapeutics. Cancer Cell *1*, 13–15.

Schindler, T., Sicheri, F., Pico, A., Gazit, A., Levitzki, A., and Kuriyan, J. (1999). Crystal structure of Hck in complex with a Src family-selective tyrosine kinase inhibitor. Mol. Cell *3*, 639–648.

Schindler, T., Bornmann, W., Pellicena, P., Miller, W.T., Clarkson, B., and Kuriyan, J. (2000). Structural mechanism for STI-571 inhibition of abelson tyrosine kinase. Science *289*, 1938–1942.

Superti-Furga, G., and Courtneidge, S.A. (1995). Structure-function relationships in Src family and related protein kinases. Bioessays *17*, 321–330.

Thomas, S.M., and Brugge, J.S. (1997). Cellular functions regulated by Src family kinases. Annu. Rev. Cell Dev. Biol. *13*, 513–609.

Van Etten, R.A. (1999). Cycling, stressed-out and nervous: cellular functions of c-Abl. Trends Cell Biol. *9*, 179–186.

Williams, J.C., Weijland, A., Gonfloni, S., Thompson, A., Courtneidge, S.A., Superti-Furga, G., and Wierenga, R.K. (1997). The 2.35 Å crystal structure of the inactivated form of chicken Src: a dynamic molecule with multiple regulatory interactions. J. Mol. Biol. *274*, 757–775.

Wisniewski, D., Lambek, C.L., Liu, C., Strife, A., Veach, D.R., Nagar, B., Young, M.A., Schindler, T., Bornmann, W.G., Bertino, J.R., et al. (2002). Characterization of potent inhibitors of the Bcr-Abl and the c-kit receptor tyrosine kinases. Cancer Res. *62*, 4244–4255.

Woodring, P.J., Hunter, T., and Wang, J.Y. (2001). Inhibition of c-Abl tyrosine kinase activity by filamentous actin. J. Biol. Chem. *276*, 27104–27110.

Xu, W., Doshi, A., Lei, M., Eck, M.J., and Harrison, S.C. (1999). Crystal structures of c-Src reveal features of its autoinhibitory mechanism. Mol. Cell *3*, 629–638.

Yamaguchi, H., and Hendrickson, W.A. (1996). Structural basis for activation of the human lymphocyte kinase Lck upon tyrosine phosphorylation. Nature *384*, 484–489.

Young, M.A., Gonfloni, S., Superti-Furga, G., Roux, B., and Kuriyan, J. (2001). Dynamic coupling between the SH2 and SH3 domains of c-Src and Hck underlies their inactivation by C-terminal tyrosine phosphorylation. Cell *105*, 115–126.

Zimmermann, J., Buchdunger, E., Mett, H., Meyer, T., and Lydon, N.B. (1997). Potent and selective inhibitors of the Abl-kinase: phenylamino-pyrimidine (PAP) derivatives. Bioorg. Med. Chem. Lett. *7*, 187–192.

Accession Numbers

Coordinates and structure factors have been deposited in the Protein Data Bank (accession codes 1OPJ [Structure A], 1OPL [Structure B], and 1OPK [Structure C]).